

Journal Pre-proof

3D-Printed Chewable *Gummies*: A Customizable Approach to Formulate Propranolol in the Paediatric Population

Costanza Fratini, Annalisa Aluigi, Mattia Tiboni, Luca Casettari



PII: S1773-2247(25)00984-0

DOI: <https://doi.org/10.1016/j.jddst.2025.107581>

Reference: JDDST 107581

To appear in: *Journal of Drug Delivery Science and Technology*

Received Date: 10 July 2025

Revised Date: 25 September 2025

Accepted Date: 27 September 2025

Please cite this article as: C. Fratini, A. Aluigi, M. Tiboni, L. Casettari, 3D-Printed Chewable *Gummies*: A Customizable Approach to Formulate Propranolol in the Paediatric Population, *Journal of Drug Delivery Science and Technology*, <https://doi.org/10.1016/j.jddst.2025.107581>.

This is a PDF file of an article that has undergone enhancements after acceptance, such as the addition of a cover page and metadata, and formatting for readability, but it is not yet the definitive version of record. This version will undergo additional copyediting, typesetting and review before it is published in its final form, but we are providing this version to give early visibility of the article. Please note that, during the production process, errors may be discovered which could affect the content, and all legal disclaimers that apply to the journal pertain.

© 2025 Published by Elsevier B.V.

3D-Printed Chewable *Gummies*:

A Customizable Approach to Formulate Propranolol in the Paediatric

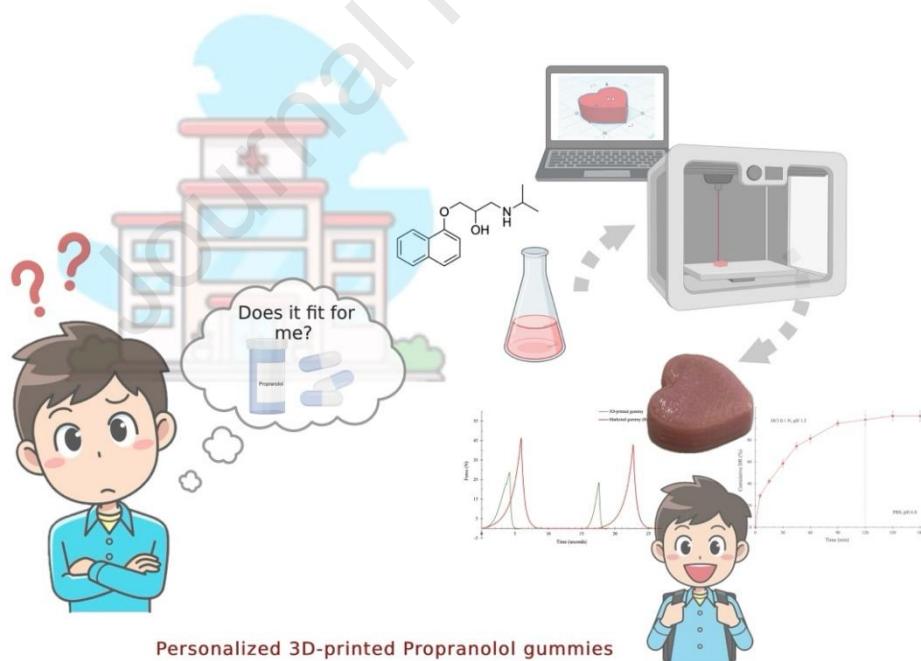
Population

Costanza Fratini^a, Annalisa Aluigi^a, Mattia Tiboni^{a*}, and Luca Casettari^a

^a University of Urbino Carlo Bo, Department of Biomolecular Sciences, School of Pharmacy, Via Ca le Suore 2,
61029 Urbino (PU), Italy

*Corresponding Author: mattia.tiboni@uniurb.it tel. +390722303336, ORCID 0000-0002-3953-4937

Graphical abstract



Personalized 3D-printed Propranolol gummies

14 **Abstract**

15 Paediatric patients, representing over 30% of the global population, continue to face a critical shortage
16 of age-appropriate pharmaceutical formulations. This gap is largely attributed to the high cost and
17 complexity of paediatric drug development, resulting in the widespread off-label use of adult
18 medications in children—an approach that compromises safety, therapeutic efficacy and adherence.
19 Conventional manufacturing methods often fail to meet essential paediatric requirements such as dose
20 flexibility, palatability, and ease of administration, all of which are pivotal for ensuring treatment
21 adherence. Providing that the European Paediatric Formulation Initiative (EuPFI) and EMA reflection
22 papers suggest that chewable dosage forms are generally acceptable starting at around age 3,
23 chewables are usually considered acceptable for children from about 3–5 years onward.

24 This study proposes a semisolid extrusion-based 3D printing methodology for the fabrication of
25 chewable paediatric dosage forms—referred to as *gummies*—incorporating propranolol
26 hydrochloride as a model hydrophilic drug commonly prescribed for cardiovascular and cardiac
27 conditions in children. A hydrogel matrix consisting of 7% w/w iota-carrageenan and 3% w/w sodium
28 alginate was optimized to ensure appropriate rheological properties, printability, and structural
29 integrity. Fourier-transform infrared (FTIR) spectroscopy confirmed the uniform distribution of the
30 active pharmaceutical ingredient within the matrix. Texture profile analysis revealed desirable
31 mechanical properties when compared to those of commercially available gummy formulations
32 (Haribo® teddy bears, Bonn, Germany). Furthermore, the printed dosage units conformed to the
33 European Pharmacopoeia quality specifications for mass uniformity and content uniformity. Notably,
34 the simplicity and scalability of the presented approach suggest its suitability for implementation in
35 both hospital and community pharmacy environments, facilitating decentralized manufacturing of
36 personalized paediatric medications.

37

38

39

40 **Keywords:** personalized medicine; additive manufacturing; propranolol hydrochloride; gummies;
41 natural excipients

42

43

Journal Pre-proof

44 1. Introduction

45 The development of age-appropriate pediatric medications remains a significant concern in the
46 pharmaceutical field. Despite children's specific physiological requirements, many commercially
47 available medications are developed with a *one-size-fits-all* approach causing dosing, acceptance, and
48 adherence to be very challenging [1–3]. Propranolol (PR) is a beta-blocking active pharmaceutical
49 ingredient (API) commonly used in children to treat conditions such as infantile hemangiomas,
50 arrhythmias, and certain cases of hypertension and migraine [4–6]. It works by reducing heart rate
51 and blood pressure and controlling abnormal blood vessel growth. In pediatric patients, the dosage is
52 typically tailored from physicians based on weight and the specific condition being treated. Usually,
53 the prescribed amounts arise around 0.5-4, up to 8 mg/kg/day divided into two or three doses and
54 gradually adjusted as needed [7]. Currently, Hemangioli[®] is the only propranolol hydrochloride liquid
55 formulation specifically developed and approved for pediatric use. It is an oral solution (3.75 mg/mL)
56 indicated for infants aged 5 weeks to 12 months with proliferating infantile hemangiomas,
57 administered twice daily with dose adjustments based on weight. However, being 40 mg tablets the
58 only other therapeutic alternative, there is a significant lack of PR-based formulations specifically
59 designed for pediatric use, which raises difficulties in ensuring accurate dosing and administration
60 for younger children (age > 3 years) that may require PR for other diseases such as arrhythmias or
61 hypertension [8]. This problem is often faced by the manipulation of already existing formulations
62 such as tablets or capsules, actions that can compromise efficacy and safety of the treatment [3]. This
63 significant gap is only one of the several examples underscoring the need for age-appropriate
64 medications to improve treatment adherence and safety in young patients.

65 In this context, 3D printing (3DP) has emerged as a revolutionizing manufacturing technology with
66 the potential to address these challenges. By allowing for an easy and precise fabrication of dosage
67 forms with desired shapes, sizes, and amount of loaded drug, 3DP offers unique opportunities to
68 produce tailored batches of medications that deal with the specific needs of single patients [9]. This

69 provides age-appropriate dosing and improvements in compliance. Moreover, the adaptability and
70 simplicity of 3DP, as well as its decentralized nature, make it suitable for integration into hospital
71 and community pharmacy settings where it enables the on-demand production of personalized
72 medications with accurate dosing tailored to individual patient needs [10].

73 Oral dosage forms are the most exploited route of administration, thanks to their convenient and easy
74 handling [11]. However, swallowing remains a concern, particularly in the paediatric population. For
75 this reason, chewable oral dosage forms are gaining a lot of interest, also being more appealing to
76 young patients and thus raising therapeutical adherence [3]. Nonetheless, one of the most persistent
77 challenges in developing chewable formulations is palatability, which significantly influences
78 acceptability. Regulatory bodies such as the European Medicines Agency (EMA) have emphasized
79 the importance of palatability testing in early stages of pediatric drug development. According to the
80 EMA guideline on pharmaceutical development of medicines for pediatric use [12], palatability—
81 defined as the overall appreciation of a medicine's organoleptic properties such as taste, texture and
82 mouthfeel—is a key determinant of acceptability. More recently, a validated composite endpoint
83 framework that integrates swallowability and palatability to assess oral formulations across pediatric
84 age groups offering a standardized approach to evaluate sensory attributes was proposed [13]. Despite
85 these advances, chewable formulations still face hurdles due to the lack of universally accepted
86 sensory testing protocols and the variability in children's taste preferences. Moreover, standardized
87 and validated tools for assessing palatability in pediatric populations are still evolving, underlining
88 the need for robust, evidence-based evaluation approaches during formulation development [14].

89 According to guidance from the European Paediatric Formulation Initiative (EuPFI) and the EMA
90 reflection paper [15], chewable dosage forms are considered suitable for pediatric use from around 3
91 years of age, with consistent acceptability generally observed in children aged 3 to 5 years. Thus,
92 Semisolid extrusion-based (SSE) 3DP technique has been recently explored to produce gummy-like
93 oral dosage forms in an easy and versatile way. The “ink” is pre-formulated usually in the form of a

94 gel or paste and subsequently loaded into the 3D printer. This allows to customize the formulation
95 according to the needs, giving the possibility to easily and quickly adjust the overall amount of API
96 in the final dosage form [16]. For instance, 3D-printed chewable formulations of lamotrigine,
97 ranitidine, ondansetron, metformin, and amoxicillin, demonstrated feasibility in dose accuracy, shape
98 personalization, and mechanical strength [17–20]. Furthermore, SSE 3DP widens the range of
99 excipients that can be employed, in respect to their rheological properties, which are fundamental
100 when considering this 3DP technique. Natural polymers such as carrageenan and sodium alginate
101 present additional advantages being biocompatible, low-toxic and versatile materials [21,22]. They
102 enhance the functionality of the dosage forms but also align with the growing demand for safer and
103 more sustainable pharmaceutical ingredients.

104 The present study aims to develop and optimize a hybrid hydrogel based on safe and generally
105 recognised as safe (GRAS) algae-derived polymers that presents enhanced and optimized rheological
106 properties for SSE 3DP. The gel matrix was employed as an alternative manufacturing way to produce
107 customizable chewable oral dosage forms containing PR_{HCl} that target the paediatric population (age
108 > 3 years old). For this reason, heart shaped gummy-like dosage forms that can be easily chewed and
109 swallowed were printed. The 3D printing “ink” was formulated to contain 4% w/w of PR_{HCl}, selected
110 as a representative dose based on concentrations commonly found in commercially available
111 formulations. However, given the ability of 3DP to precisely adjust the amount of active
112 pharmaceutical ingredient (API) in each dosage unit by simply modifying the amount of extruded
113 material during the printing process, different design dimensions were produced to demonstrate the
114 versatility of the manufacturing process. This enables accurate, patient-specific dose customization
115 without the need for dosage manipulation such as tablet splitting, crushing, or dissolving—procedures
116 that are often associated with dosing inaccuracies, drug loss, and safety concerns [10]. The resulting
117 3D-printed *gummies* were tested in terms of quality standards required by the European
118 Pharmacopoeia. Moreover, the uniformity of drug distribution within and across individual dosage

119 forms was assessed, alongside evaluations of the solid-state properties, mechanical strength, and drug
120 release behaviour of the formulations.

121

Journal Pre-proof

122 2. Materials and methods

123 2.1. Materials

124 Sodium Alginate (SA, Protanal PC 6850, 400-600 cps) was obtained from Biochim (Italy), while iota-
125 Carrageenan (ι -K, 60072/24) from Java Biocolloid Europe s.r.l. (Italy). Propranolol hydrochloride
126 (PR_{HCl}) and saccharin sodium (E954) were acquired from Farmalabor (Italy). Calcium Chloride
127 (CaCl_2) was purchased from Carlo Erba reagents (Italy).

128

129 2.2. Hydrogel formulations

130 Different hydrogel formulations were prepared as described in Table 1. First, a 10 % w/w of SA or ι -
131 K were examined. Subsequently, a combination of the two polymers for an overall amount of 10%
132 w/w was evaluated. All hydrogels comprise of 0.5 % w/w of saccharin sodium (E954) and 4% of
133 propranolol hydrochloride (PR_{HCl}) that were first dissolved in the water medium. ι -K was added in
134 Milli-Q® water at 70 °C and magnetically stirred (600 rpm) until complete dissolution, then SA was
135 added to the system and stirred until cooling at room temperature (25 °C). All the formulations were
136 left overnight to enable complete gel formation.

137

138 2.3. Miscibility test

139 The miscibility of the two matrix polymers was assessed through the comparison of theoretical and
140 experimental viscosities (η) of the resulting hydrogels. Specifically, evaluating the flow curve
141 (operating parameters are described in section 2.4) of each material and of the mixture of the two at
142 the considered concentrations. *Eq. 1*, also known as logarithmic mixing rule, was employed to obtain
143 the theoretical viscosity [23], while, for the experimental one, a low and fixed value for the shear

144 strain (γ) was determined and the related viscosity recorded. Both unloaded and drug-loaded
 145 hydrogels were evaluated. Analysis was carried out in triplicate.

$$146 \quad \ln \eta_T = (\omega_{t-K} \cdot \ln \eta_{t-K}) + (\omega_{SA} \cdot \ln \eta_{SA}) \quad Eq. 1$$

147

148 Where η_T represent the theoretical viscosity, ω_{t-K} and ω_{SA} the weight fraction, η_{t-K} and η_{SA} the
 149 experimental 10 % w/w t-K and 10 % w/w SA hydrogel viscosities, respectively.

150

151 **2.4. Rheological characterizations**

152 The rheological properties of hydrogels significantly affect printability, and are, therefore, important
 153 parameters to determine [24]. Rheological analysis was performed using a MCR 302e rheometer
 154 (Anton Paar, Austria) provided with a plate-plate probe (PP, 25mm \varnothing , gap 1 mm), at a controlled
 155 temperature of 25 °C. All the analysis were performed in triplicate. *Flow curve*: the shear rate ($\dot{\gamma}$) was
 156 set in the range of 0.01–10³ s⁻¹, logarithmic ramp. Shear stress (σ) and viscosity (η) were recorded to
 157 determine the flow behaviour of the material during the extrusion stage. The *shear recovery test*,
 158 specifically the three-interval thixotropy test (3ITT) procedure is shown in Table 2. The shear
 159 recovery percentage was obtained by the steady-state viscosity of step 3 divided by the steady-state
 160 viscosity of step 1 and used to determine the thixotropic behaviour of the hydrogels. *Amplitude sweep*:
 161 oscillating strain range was set at 0.01–100 %, logarithmic ramp, and fixed the angular frequency (ω)
 162 at 10 rad/s. Storage (G') and loss (G'') modulus were recorded and used to determine the linear
 163 viscoelastic region (LVR), the yield and flow point (loss of linearity and crossover point,
 164 respectively). *Frequency sweep*: oscillating strain was fixed at 0.1 % and 1 % for drug-loaded and
 165 unloaded hydrogels, respectively with an angular frequency (ω) range of 300 - 0.03 rad/s, logarithmic
 166 ramp.

167

168 **2.5. Design and 3D printing parameters**

169 A heart-shaped *gummy* was 3D printed using a BioX 3D biprinter (Cellink, Sweden). The design
170 was obtained with a free computer aided design (CAD) software (Tinkercad®, Autodesk Inc, USA).
171 Different design dimension (15x15x5, 12x12x4, 10x10x3, 8x8x2 mm) were printed to obtain different
172 loading amounts of the API. A 3 mL syringe equipped with a plastic nozzle 22G (0.4 mm) was filled
173 with the hydrogel and loaded into the head of the printer. Printing was carried out at room temperature
174 (RT). The infill was set at 80% and the geometry rectilinear with a layer height of 0.4 mm. Printing
175 speed was set at 5 mm/s and the pressure of ~ 35 kPa and ~ 85 kPa for the drug-loaded and unloaded
176 hydrogels, respectively. After printing, the *gummy* was cross-linked in a 1 M CaCl₂ bath for 5 minutes
177 and then let dry at room temperature for 4 hours until packaging the single units in sealed bags under
178 vacuum.

179

180 **2.6. Fourier-transform infrared spectroscopy (FTIR) analyses**

181 The raw materials and drug-loaded and unloaded 3D-printed *gummies* were analyzed with FTIR
182 (ATR-FTIR, Spectrum Two, Perkin Elmer, USA) to evaluate any possible interaction or chemical
183 degradation within the materials and the API distribution. Each tested dosage form was divided into
184 three sections for a total of three dosage units chosen randomly from a printed batch. Transmittance
185 (%) was recorded in the wavelength interval of 4000-400 cm⁻¹. Samples underwent 64 scans with a
186 resolution of 4 cm⁻¹. To evaluate the homogeneous distribution of PR_{HCl} a single dosage form was
187 divided into three pieces (A, B and C), the same method was used on a total of three dosage units.
188 The samples were analysed at the FTIR and intensities of peaks related to the drug (1105 cm⁻¹ and
189 769 cm⁻¹) were compared. For clearer results, the *gummies* were previously let overnight to dry at
190 room temperature. Air was used as the background for each analysis.

191

192 **2.7. Differential scanning calorimetry (DSC) and thermogravimetric analyses**

193 The thermal profile of the pure drug, raw excipients and the 3DP *gummies* (both freshly made and
194 stored under vacuum packages for one week) was investigated through DSC (DSC 6000, Perkin
195 Elmer, USA) and TGA (TGA 4000, Perkin Elmer, USA). Specifically, for DSC measurements,
196 approximately 5 mg of sample were placed in aluminium pans and heated up from 30 °C to 200 °C
197 at 10 °C/min while for TGA, samples were subjected to a heating ramp from 30 °C to 500 °C at 10
198 °C/min. Nitrogen flow rate was kept at 30 mL/min. Analyses were carried out in triplicate.

199

200 **2.8. Powder X-ray diffraction (PXRD) analyses**

201 PXRD spectra of the pure drug, raw excipients and the 3DP *gummies* (both freshly made and stored
202 under vacuum packages for one week) were collected. For each *gummy*, three random sections were
203 prepared. Measurements were carried on a Miniflex benchtop diffractometer (Rigaku, Tokyo, Japan),
204 using Cu-K α radiation ($\lambda = 1.5418 \text{ \AA}$) with a D/teX Ultra2 detector. All the measurements were
205 conducted in the 2θ range of 5-50 ° with a step size of 0.01 ° and a scan speed of 2 °/min. The analyses
206 were performed in triplicate.

207

208 **2.9. Determination of mass uniformity, content uniformity, and drug loading**

209 To assess the mass uniformity of the printed dosage forms, twenty of these were measured after cross-
210 linking and the average weight calculated. According to the European Pharmacopoeia (XI ed.), no
211 more than two dosage forms should vary $\pm 5 \%$ from the average. Content uniformity and the actual
212 amount of API loaded in the 3D-printed dosage forms were evaluated dissolving 10 *gummies* in PBS
213 pH = 6.8 and the resulting amount of loaded PR_{HCl} studied at the UV-Vis (UV-1900i, Shimadzu,
214 Japan) at a wavelength $\lambda_{\max} = 289 \text{ nm}$. A calibration curve was previously performed with an $R^2 =$
215 0.9996. As reported in the European Pharmacopoeia XI ed., the content of API should not deviate

216 more than $\pm 15\%$ from the average. PR_{HCl} content was also assessed at the end of the storage period
217 (one week under vacuum conditions).

218

219 **2.10. Drug release studies**

220 Drug release studies for all the design variations were carried out adapting the dissolution test for oral
221 dosage forms described in the European Pharmacopoeia (XI ed.). A PTWS 120D Dissolution
222 apparatus (Pharma Test, Germany) equipped with a basket stirring tool was employed. Stirring was
223 fixed at 75 rpm and the temperature kept at 37°C. Various pH media were used to simulate the
224 physiological conditions. To mimic the acidity of the stomach, the samples were placed in 375 mL of
225 HCl 0.1N pH 1.2 for the first two hours. After that, 125 mL of Na₂HPO₄ 0.2M were added, and the
226 pH increased to 6.8 with the least amount of NaOH 2M to resemble the transit to the intestine. Sink
227 conditions were ensured for the analysis. For the first hour, time points were taken at 5, 15, 30, 45,
228 and 60 minutes, and then every 30 minutes until the test was over. At each time point, 1 mL samples
229 were collected and replaced with fresh media. Before being placed in the basket tool, the *gummies*
230 were randomly fragmented in 10 pieces with a scalpel to mimic the masticatory process. Quantitative
231 studies were carried out employing a UV-Vis spectrophotometer as previously described (section 2.9).
232 Analysis was performed in triplicate.

233

234 **2.11. Mechanical properties of the *gummies***

235 A Texture Profile Analysis (TPA) was carried out on the 3D-printed *gummies* and then compared to
236 conventional marketed gummy bears (Haribo® teddy bears, Bonn, Germany). The test was run using
237 a Texture Analyzer, TA.XT plus, (Stable Micro Systems, UK) equipped with a loading cell of 50 Kg
238 and a compression probe (P/20 Ta.Tx, 20 mm diameter). A two-cycle compression was performed.
239 The strain and trigger force were set at 60 % and 5 g, respectively and test speed set at 1 mm/s. A

240 second compression was performed after 5 seconds from the first. Parameters such as hardness (N),
241 cohesiveness, adhesivity and gumminess (N) were calculated using Eq. 2-4. Analyses were carried
242 out in triplicate.

$$243 \quad \text{Hardness (N)} = F_1 \quad \text{Eq. 2}$$

244 Where F_1 is the max force registered after the first compression.

$$245 \quad \text{Cohesiveness} = A_2/A_1 \quad \text{Eq. 3}$$

246 Where A_2 and A_1 are the positive areas under the curve of the second and first peak of compression,
247 respectively.

$$248 \quad \text{Gumminess (N)} = \text{Hardness} * \text{Cohesiveness} \quad \text{Eq. 4}$$

249

250 **2.12. Stability studies**

251 The dosage form's stability was evaluated through time both assessing the weight, water loss (WL),
252 and the consistency of the mechanical properties. The 3D-printed *gummies*, that were stored at room
253 temperature in single packages under vacuum, were analyzed at different time points: 24, 48, 72 h,
254 and after 7 days from manufacturing. To assess the mechanical characteristics the test was carried out
255 as previously described (section 2.10), while for WL, Eq. 7 was used. Each analysis was carried out
256 in triplicate.

$$257 \quad \text{WL (\%)} = [(m_0 - m_x)/m_0] * 100 \quad \text{Eq. 7}$$

258 Where m_0 and m_x are the dosage form's mass after printing and at each time point, respectively.

259

260 **2.13. Statistical analysis**

261 All results are shown as mean \pm standard deviation (SD) which was calculated from the values of at
262 least three independent tests. Data was analysed using a t-test. The criterion for statistical significance
263 was $p < 0.05$.

264

265

Journal Pre-proof

266 3. Results

267 3.1. Polymer miscibility evaluation

268 Since the selected hydrogels consist of a combination of SA and ι -K, the miscibility of the two
269 polymers was evaluated. Considering the flow curve obtained through rheological analyses (section
270 3.2.1), calculated and experimental viscosities of the complex systems, at each concentration, were
271 compared and are shown in Fig. 1. A positive deviation from the theoretical values was seen for all
272 the considered combinations, meaning that a good miscibility between the two polymers exists. When
273 PR_{HCl} is added to the system, a negative deviation from the theoretical values is observed. Meaning
274 that a reduction in the miscibility occurs. This event can be explained because of the interactions
275 occurring among the API, SA and ι -K, probably changing the way SA and ι -K interact with one
276 another. During the gelation process, ι -K initially undergoes transitions from coil to helix until
277 forming double helix aggregations. Strong and compact three-dimensional networks are developed
278 when SA readily entangles with ι -K thanks to a high degree of hydrogen bonding [25,26]. Positively
279 charged amino groups, present in the molecules of PR_{HCl} , interact with sulfonated groups of ι -K, thus
280 affecting the intensity and number of the intermolecular bonds between SA and ι -K [26,27] and
281 resulting in an increase of the mobility and space among the polymers' chains.

282

283 3.2. Rheological characterization

284 Particularly in the context of hydrogels, rheology plays a vital role in the field of extrusion-based 3D
285 printing. Rheological features of the material significantly impact the response to stress and strain,
286 extrudability and shape retention, thus the overall manufacturing process [24,28]. Optimization can
287 be performed once having evaluated parameters such as shear thinning behaviour, thixotropy, and
288 viscoelasticity of the formulation. The way the material behaves, both during and after the printing
289 process, are greatly influenced by these factors. The ease with which the substance passes through

290 the nozzle is influenced by viscosity and shear thinning, while the material's response to and recovery
291 from stress during and after deposition is determined by its viscoelasticity.

292

293 **3.2.1. Shear analyses**

294 Fig. 2-A shows the recorded viscosity plotted against the shear rate. Although all the tested
295 formulations (F1:F5), both with and without PR_{HCl}, presented a shear thinning behaviour, this was
296 not sufficient to determine the good printability of the material. When the fluid at rest is subjected to
297 an external force, its viscosity should decrease rapidly allowing for easy extrusion through a small-
298 diameter hole. Indeed, all formulations resulted to be extrudable at an acceptable pressure (Section
299 3.3, Fig. 3-A). However, when the force is removed, the viscosity of the material should rapidly
300 recover. This feature is crucial to maintain the shape and integrity of the extruded material, strongly
301 affecting the layer-by-layer construction. Thixotropy is a time-dependent rheological property that
302 describes how reversible the changes occurring in the sample's internal structure are [24]. For this
303 reason, the three-interval thixotropy test (3ITT), provides essential details regarding the recovery
304 rates following extrusion [29]. As reported in Fig. 2-B to simulate the three main steps of the 3D
305 printing process, the viscosity was examined over time as a function of the shear rate. Representing
306 the rest state before printing, extrusion, and recovery steps. Excepting F1 (red line), all the
307 formulations showed good recovery profiles after being subjected to high shears, reaching < 55 %
308 viscosity recovery within 30 s. This ensures shape fidelity after extrusion without excessive spreading
309 or deformation of the deposited material during the 3D printing process.

310

311 **3.2.2. Oscillatory analyses and viscoelastic properties**

312 Viscoelasticity provides important information about the solid-like or liquid-like properties of the
313 sample by evaluating the material's storage modulus (G') and loss modulus (G''). Amplitude sweeps

314 tests are performed subjecting the system to a range of deformations at a fixed oscillatory frequency.
315 The linear viscoelastic region (LVR), indicating the range in which oscillatory tests can be performed
316 without destroying the internal structure of the sample, is evaluated and information about the
317 viscoelastic nature of the samples obtained. Solid-like structures, thus those considered more suitable
318 for 3D printing, should present a $G' > G''$. Other than F1 (red line), which shows a $G'' > G'$ (Fig 2-
319 C), all the tested formulations (Fig. 2-C and Fig. 2-D) both unloaded and loaded with PR_{HCl} , can be
320 considered printable in terms of layer-by-layer deposition showing a solid-like behaviour ($G' > G''$)
321 and a crossover point. F5 (black line), resulted to be the stiffest sample, with the highest value for G'
322 ($G' = 8100$ Pa). F2-F5 also present a yield point, which can be graphically described as the point at
323 which the curve deviates from linearity, indicating the stress at which the *ink* transitions from a solid-
324 like to a liquid-like state. Thus, the stress necessary to be applied for the material to start flowing.
325 Frequency sweeps tests, shown in Fig. 2-E and Fig. 2-F, involve strain amplitude that is kept constant
326 and within the LVR, while the oscillation frequency is increased. Through this test a better
327 understanding of the internal structure of the system and its time-dependent behaviour, in a non-
328 destructive range, is made possible. High frequencies represent short-term behaviours, such as mixing
329 or extrusion while low frequencies represent long-term behaviours such as settling [24,30]. For gel-
330 like materials both G' and G'' should stay parallel across the overall frequency range. This indicates
331 that the material maintains consistent. This was observed for all the formulations (with and without
332 PR_{HCl}), apart from F1 (red line). Suggesting that a higher concentration of ι -K in the mixture can
333 provide a more gel-like structure, thus more suitable *inks* for the 3D printing process.

334

335 3.3. 3D printing and customization

336 Fig. 3-A presents a visual comparison of all the studied formulations at the 3D printer, in terms of
337 extrudability and printability. As already underlined from the rheological studies, when formulated
338 alone (F5), ι -K provides hydrogels that are very elastic and solid-like, with a very high G' , resulting

339 in a brittle and rough material that does not provide continuity during extrusion, while SA alone (F1)
340 forms a structured system that is more liquid-like ($G'' > G'$) thus not suitable for the layer-by-layer
341 process. The most suitable combination of the two natural polymers for 3D printing was determined
342 to be SA/ ι -K in a 3:7 (F4) based on best extrudability, printability and shape fidelity results. Following
343 the printing process, the constructs underwent ionic cross-linking and were subsequently air-dried for
344 four hours to enhance the structural integrity of the final 3D-printed dosage forms. In Fig. 3-B is
345 represented the CAD design of the *gummy* meanwhile, in Fig. 3-C are reported images of the final
346 3D-printed *gummies* using the selected most suitable formulation (F4) and showing a close-up to the
347 layering of the material. Pictures were taken at the optical microscope after cross-linking and drying.
348 Moreover, to demonstrate the versatility of the manufacturing process in enabling customization and
349 personalization, gummy formulations were successfully printed in a range of design dimensions
350 ($15 \times 15 \times 5$ mm, $12 \times 12 \times 4$ mm, $10 \times 10 \times 3$ mm, and $8 \times 8 \times 2$ mm), as illustrated in Fig. 3-D. The printing
351 process was notably efficient, with production times ranging from 12 minutes for the largest unit to
352 just 1.5 minutes for the smallest. As shown in Table 3, the final printed dimensions closely matched
353 the intended design specifications, confirming the precision and reproducibility of the technique.

354

355 **3.4. Fourier-Transform Infrared Spectroscopy (FTIR)**

356 ATR-FTIR was employed to investigate the chemical interactions among the formulation's
357 components and to confirm the homogeneous distribution of PR_{HCl} in the dosage form. For this
358 reason, the raw materials (SA, ι -K, E954, and PR_{HCl}), the unloaded and loaded 3D-printed *gummies*
359 were analyzed. Results are shown in Fig. 4-A. Given the structural analogies, SA and ι -K show similar
360 main signals: a broad band in the range of $3600-3100$ cm^{-1} is observed, attributed to the stretching
361 vibration of OH groups, weakened in intensity due to intermolecular hydrogen bonds between the
362 polymer chains [31]. At 1593 cm^{-1} and 1402 cm^{-1} , SA shows the characteristic peaks attributed to the
363 stretching vibration of the carboxyl group (COOH), while an intense, broad absorption band at $1150-$
364 1000 cm^{-1} corresponds to the stretching vibrations of C-O-C bonds of the glycosidic rings typical of

365 polysaccharides[31], present both in SA and ι-K. Significant for ι-K are the asymmetric and
366 symmetric stretching vibrations of the sulphate groups generally observed by three bands at 1220,
367 1157 and 574 cm^{-1} [32,33]. In the FTIR spectrum of E954, the broad band around 3250 – 3550 cm^{-1}
368 is attributed to the stretching vibrations of NH groups present in the benzisothiazole ring while the
369 splitted peak at 1632 cm^{-1} correspond to the C=O vibrations [34]. Bands corresponding to asymmetric
370 and symmetric stretches of the SO₂ group are observed at 1255 and 1144 cm^{-1} [34,35]. PR_{HCl} shows
371 peaks related to NH stretching of the secondary amine and CH stretching vibrations peaks attributed
372 to the methyl groups in the molecule around 3300-2800 cm^{-1} . In addition, the corresponding peaks at
373 1105 cm^{-1} and 769 cm^{-1} are observed for C-O-C stretching in the aryl alkyl ether group and α-
374 substituted naphthalene [36,37].

375 The FTIR spectra of 3D-printed *gummies* display similarities with the ones obtained for the starting
376 materials. Slight shifts or weakening of the peaks are attributed to the engagement of the functional
377 groups into intermolecular interactions and due to the cross-linking with CaCl₂. SA's peaks shown at
378 1593 and at 1402 cm^{-1} which are attributed to the carboxyl groups vibrations are indeed shifted to
379 1634 and 1421 cm^{-1} respectively, which can be associated with the presence of calcium ions, from
380 the cross-linking agent, forming "egg-box" structures among SA and ι-K chains. The term "egg-box
381 structure" refers to a molecular arrangement commonly observed in polysaccharide gels, particularly
382 those involving alginate and other anionic polymers. In this configuration, divalent cations such as
383 calcium (Ca²⁺) interact with the carboxylate groups of the polymer chains, creating cross-links that
384 resemble the compartments of an egg box. This organized network stabilizes the gel matrix and
385 contributes to its mechanical strength and elasticity [31]. Overall, the FTIR analysis revealed that no
386 new peaks were generated, and no significant peaks disappeared in the optimized formulation. This
387 suggested that no degradation or instability occurred during formulation.

388 As a final step in the FTIR analysis, the uniform distribution of PR_{HCl} within the 3D-printed dosage
389 forms was assessed by examining the spectra from three distinct sections (A, B, and C) of a single

390 unit containing the active pharmaceutical ingredient (API), as well as from three separate dosage
391 units. As illustrated in Fig. 4-B, all spectra exhibited the characteristic peaks of PR_{HCl} with
392 comparable intensities, indicating consistent API presence throughout the samples. A maximum
393 transmittance variability of 10% was observed across the different sections of the individual unit and
394 among the three units (Sample 1, Sample 2, and Sample 3), as visualized in the 3×3 distribution
395 spectral map presented in Fig. 4-C.

396

397 **3.5. Solid state characterization**

398 Thermal analyses (DSC and TGA) and powder x-ray diffraction (PXRD) were carried out to evaluate
399 the crystalline form of the drug in the 3D printed *gummies* both freshly made and after one week of
400 storage under vacuum conditions.

401 TGA thermograms (Fig. 5-B) illustrate the thermal behaviour of the materials studied up to 500 °C.
402 Within this temperature range, only PR_{HCl} underwent complete thermal degradation, occurring at
403 315.57 °C. In contrast, E954 demonstrated thermal stability, aside from a 10% weight loss attributed
404 to water evaporation between 58 °C and 150 °C [38]. SA and ι -K, which share structural similarities,
405 exhibited comparable thermograms: an initial 10–15% weight loss between 30 °C and 130 °C due to
406 moisture release, followed by a more pronounced degradation associated with structural breakdown
407 at 259.81 °C and 279.86 °C, respectively [39]. Both fresh and stored 3D-printed *gummies* exhibited
408 thermal behaviour similar to SA and ι -K, which are the primary matrix excipients. In contrast, a more
409 pronounced weight loss of approximately 40–45% was observed between 30 °C and 140 °C,
410 attributed to the higher moisture content.

411 DSC thermograms of the pure drug and excipients were initially recorded. As illustrated in Fig. 5-A,
412 PR_{HCl} displays a sharp and intense endothermic peak at 169.21 °C, corresponding to its melting [40].
413 E954, which exists in multiple hydrated forms, exhibits an initial dehydration peak followed by a

414 low-intensity endothermic signal around 75.31 °C, attributed to a phase transition. This is
415 subsequently followed by a second dehydration event at 130.09 °C. Although the melting point of
416 E954 is reported to be approximately 360 °C [38] it was not observed within the selected temperature
417 range of the analysis. SA and ι -K, exhibit a broad endothermic event between 50 °C and 150 °C,
418 attributed to moisture loss. Consistent with TGA results, both fresh and stored 3D-printed *gummies*
419 display thermograms resembling those of the two main polymers, but with a broader and more intense
420 endothermic signal in the same temperature range, reflecting their higher water content.

421 To further assess the crystallinity of the drug within the 3DP dosage forms, PXRD analyses were
422 conducted. The diffraction patterns of pure PR_{HCl} and E954 confirm the high crystallinity of these
423 raw materials, as evidenced by distinct peaks at 2θ values of 8.33°, 12.70°, 12.80°, 16.67°, and 25.03°
424 for PR_{HCl}, and 6.12°, 12.21°, 24.51°, and 30.79° for E954 (Fig. 5-C), in agreement with previously
425 reported data in the literature. [38,40]. SA and ι -K predominantly exhibit an amorphous nature, as
426 evidenced by the absence of distinct crystalline peaks in their PXRD patterns. However, two
427 diffraction peaks at 2θ values of 28.42° and 40.58° are observed for ι -K, consistent with previous
428 reports in the literature [41,42]. These peaks are primarily attributed to the presence of inorganic
429 impurities within the sample. No distinct diffraction peaks were detected in either the freshly prepared
430 or stored 3D-printed *gummies*, indicating that the formulation successfully achieved complete
431 amorphization of the crystalline drug and excipients. Notably, no recrystallization was observed over
432 a one-week storage period. However, three weak peaks were present that closely align with known
433 E954 diffraction values. These may be attributed to incomplete dissolution of the excipient during
434 formulation. Minor peak shifts could result from the dispersion of E954 within the predominantly
435 amorphous matrix. PXRD data collected from stored *gummies* sections confirmed that the drug
436 remained in its amorphous state.

437

438 3.6. Mass uniformity, content uniformity, and drug loading

439 In accordance with the guidelines for oral dosage forms outlined in the European Pharmacopoeia (XI
440 ed.), twenty 3D-printed units were weighed following the cross-linking process. Of these, only two
441 units deviated beyond the primary limit of $\pm 5\%$; however, both remained within the secondary
442 acceptance range of $\pm 10\%$, thereby fulfilling the criteria for mass uniformity. Average weight was
443 991.55 ± 8.54 mg. For content assessment, 10 units were disintegrated and completely dissolved to
444 calculate the real amount of API loaded. No dosage form was found out of the given limits, indeed
445 the average amount of drug loaded was of 40.04 ± 1.35 mg. Results are shown in Fig. 6, A-B and
446 Table 3. Moreover, following one week of storage under vacuum conditions, the active
447 pharmaceutical ingredient (API) content remained stable, with no significant degradation observed
448 (39.76 ± 1.08 mg).

449

450 3.7. Drug release

451 Dissolution studies were carried out on fragmented *gummies* to study the release profile of PR_{HCl} from
452 the matrix residues after swallowing the chewed dosage form. Before the dissolution test,
453 fragmentation of the *gummies* was conducted to simulate the masticatory process that occurs before
454 swallowing. Given that mastication is variable and patient-dependent, it cannot be precisely
455 reproduced in vitro. To approximate this variability, each *gummy* was divided into 10 fragments of
456 non-uniform size, thereby introducing a degree of randomness intended to enhance the relevance of
457 the dissolution results. The dissolution profiles of all design variations were systematically evaluated.
458 The release kinetics remained consistent, indicating reliable drug release behaviour related to the
459 polymer matrix. Despite the different drug loads and dosage unit's dimensions, it was observed that
460 release rates were not predictable, this might be related to minimization of the effect of surface area
461 to volume ratio due to fragmentation prior testing [43]. After 5 min a 25.44 ± 2.67 % of released drug
462 was measured, reaching 75.27 ± 4.80 % after 60 min. The drug release profile of the dosage units is
463 shown in Fig. 6-C. The common mechanism for drug release of an API from a biodegradable

464 polymeric delivery system, as it is in this case, is usually a combination of diffusion and degradation
465 processes [44]. Drug release kinetics are affected by several factors (*e.g.* drug-related, polymer-
466 related, and formulation variables) that are considered when fitting the dissolution results to
467 mathematical models. Mathematical modelling that was performed on the *gummy*'s drug release
468 profile suggested that it was best explained by Higuchi's equation ($R^2 = 0.9937$). Indeed, a complete
469 release of the drug was observed although residues of the chewed *gummy* were still not completely
470 dissolved, suggesting that diffusion of PR_{HCl} through the matrix was the main driving force of the
471 release.

472

473 **3.8. Mechanical properties**

474 To assess the mechanical performance of the 3D-printed *gummies*, a Texture Profile Analysis (TPA)
475 was conducted (Fig. 7-A). Key parameters including hardness (N), cohesiveness, and gumminess (N)
476 were derived from the force–time curves and compared with those obtained from commercially
477 available chewable gummy formulations (Haribo[®] teddy bears, Bonn, Germany) (evaluated under
478 identical TPA conditions) that were considered as a “model”. The comparative results are presented
479 in Table 4. For chewable dosage forms, it is essential to achieve a balance between sufficient softness
480 to ensure ease of mastication and adequate mechanical strength to withstand handling, packaging,
481 and transportation without compromising integrity. The 3D-printed *gummies* exhibited lower
482 hardness than that observed for marketed products indicating that the printed formulation possess
483 suitable ease of chew for paediatric use. Cohesiveness, defined as the capacity of the dosage form to
484 resist a subsequent deformation during Texture Profile Analysis (TPA), was found to be lower
485 compared to the reference model. This reduction is attributed to diminished elasticity, which is highly
486 dependent on the formulation components. Nevertheless, the gummy formulations demonstrated
487 structural integrity by withstanding a second deformation without exhibiting any macroscopic failure
488 as also observable from the graphs in Fig. 7-A.

489

490

3.9. Stability studies

491 Vacuum packaging was selected to prevent excessive drying of the dosage form (52.54 ± 2.61 %
492 water content after 4h drying) and subsequent hardening, thus ensuring the preservation of
493 mechanical properties for administration. Following seven days of storage, the 3D-printed *gummies*'
494 stability over time was assessed. At each time point, the mechanical properties, weight, and water
495 loss (%) were evaluated. During storage, the percentage of humidity, thus the elasticity and hardness
496 of the dosage forms maintained consistent. The gumminess was therefore deemed satisfactory for the
497 overall period. Fig. 7, B-E display the trend of weight, water loss and mechanical characteristics over
498 time.

499

500

501

502

503

504 4. Discussion

505 Sodium alginate (SA) is a linear polysaccharide derived from brown seaweed, composed of β -D-
506 mannuronic acid and α -L-guluronic acid moieties. It is a well-known and widely employed material
507 for 3DP due to its high and easy room temperature gelation properties, biocompatibility, low toxicity,
508 and wide range employment in food preparations [21]. However, when formulated alone its
509 printability is not optimal and often requires additional rheological modifiers to provide an extruded
510 material that has high printing resolution and shape fidelity [45]. Carrageenan (K), also extracted
511 from algae, consists mainly of sulphated galactans. There are different types of carrageenan, kappa
512 (κ), iota (ι), and lambda (λ) which differ in their sulphate content and gelling behaviour [22]. When
513 formulated alone, ι -K provides hydrogels that are very elastic and solid-like, for this reason a
514 combination of ι -K and SA was used in this study to obtain a complex hydrogel with tuneable
515 viscosity and optimized rheological properties for additive manufacturing application [46]. When
516 combined, SA and K can form a crosslinked gel network through hydrogen bonding and ionic
517 interactions thanks to the high content of carboxyl groups in SA and hydroxyl groups in K. The
518 interactions lead to a compact network enhancing the stability and mechanical properties of the
519 resulting gels [47,48]. Due to its rapid solubility in water and minimal-temperature processing
520 requirements, the formulation process is both straightforward and time-efficient, making it highly
521 suitable for small-scale, on-demand manufacturing. This is particularly advantageous in hospital
522 pharmacy settings, where the ability to prepare personalized therapies quickly is essential for meeting
523 patient-specific needs. Moreover, the resulting hydrogel may offer compatibility with a wide range
524 of hydrophilic active pharmaceutical ingredients (APIs), providing valuable flexibility in drug
525 loading and enabling tailored dosage customization. Moreover, sodium saccharine (E954) was chosen
526 as sweetener to reduce the bitter taste of the selected API given the possibility of adding a very small
527 amount to the formulation thanks to its high sweetening power [49,50]. Indeed, each dosage form
528 presents a very low amount of E954, lower than the accepted daily intake ADI defined by the FDA

529 of 9 mg/kg/day [51]. However, its use can be further optimized through the incorporation of additional
530 taste-masking agents or alternative sweeteners. 4% w/w of PR_{HCl} was added to the most suitable
531 formulation (F4) with the advantage that, by 3DP, the amount of API per dosage form can be easily
532 customized, according to the patient's needs, by modifying the dimension and weight of the dosage
533 unit. Importantly, the study highlights the versatility of SSE-3DP for personalized medicine. The
534 successful fabrication of *gummies* in various dimensions—from 15×15×5 mm to 8×8×2 mm— and
535 drug contents—from 40 mg to 4mg—demonstrates the adaptability of the process to patient-specific
536 dosing needs. The close match between CAD designs and final printed dimensions, along with
537 efficient production times, underscores the precision and reproducibility of the technique. These
538 findings align with recent literature emphasizing the potential of extrusion-based 3D printing to
539 overcome the limitations of conventional dosage forms by enabling on-demand customization and
540 scalable manufacturing [19,20,52]. Such capabilities are particularly valuable in paediatric care,
541 where dose flexibility and ease of administration are paramount. Characterization of the produced
542 dosage forms provided insights into the molecular interactions and distribution of components within
543 the 3D-printed formulations and the uniform distribution of PR_{HCl} was further confirmed by
544 consistent spectral profiles across multiple sections and units, with transmittance variability
545 remaining below 10%. This supports the homogeneity of the drug within the matrix, a critical factor
546 for dose accuracy and therapeutic reliability in personalized dosage forms. These findings reinforce
547 the utility of FTIR as a non-destructive tool for verifying component integrity and spatial uniformity
548 in 3D-printed pharmaceutical systems [53,54]. The evaluation of mass and content uniformity
549 confirmed the reliability and reproducibility of the 3D printing process for personalized dosage forms.
550 In accordance with the European Pharmacopoeia (XI ed.), the printed gummies met the acceptance
551 criteria for mass uniformity emphasizing the importance of in-process control and quality assurance
552 in 3D-printed pharmaceuticals [17,18,55,56].

553

554 5. Conclusions

555 This study successfully demonstrated the development of a customizable, pediatric-friendly oral
556 dosage form using semi-solid extrusion (SSE) 3D printing (3DP) technology. By optimizing the
557 polymer matrix composed of natural excipients such as sodium alginate and ι-carrageenan, a suitable
558 formulation was identified that balanced printability, mechanical integrity, and drug release
559 performance. Rheological analysis confirmed that the selected hydrogel exhibited favorable
560 rheological properties for additive manufacturing providing reliable extrusion and shape fidelity.
561 FTIR and PXRD analyses verified the homogeneous and amorphous dispersion and chemical stability
562 of propranolol hydrochloride (PR_{HCl}) within the matrix, with no signs of degradation or
563 recrystallization over short-term storage. The printed gummies met Pharmacopoeial standards for
564 mass and content uniformity, and dissolution testing revealed consistent, diffusion-driven drug
565 release best described by Higuchi kinetics. Mechanical profiling showed that the dosage forms were
566 softer and more chewable than commercial references (*e.g.*, Haribo® teddy bears), while maintaining
567 sufficient resilience for handling and administration. Stability studies further confirmed the
568 preservation of texture and drug content in packages sealed under vacuum conditions. Altogether,
569 these findings support SSE-3DP as a promising platform for producing age-appropriate, personalized
570 dosage forms that meet both pharmaceutical quality standards and patient-centric design
571 requirements. This approach holds particular promise for pediatric populations, where flexibility in
572 dosing, ease of administration, and improved compliance are essential.

573

574 Funding

575 This work has been funded by the European Union - NextGenerationEU, Mission 4, Component 2,
576 under the Italian Ministry of University and Research (MUR) National Innovation Ecosystem grant
577 ECS00000041 - VITALITY – CUP H33C22000430006

578 Costanza Fratini acknowledge the European Union - NextGenerationEU, Mission 4, Component 1,
579 under the Italian Ministry of University and Research (MUR) PNRR D.M. 118/2023 for the PhD
580 Scholarship

581 Author contributions: CRediT

582 **Costanza Fratini:** Methodology, Investigation, Formal analysis, Data curation, Writing – original
583 draft. **Annalisa Aluigi:** Methodology, Data curation, Writing – review & editing. **Mattia Tiboni:**
584 Conceptualization, Supervision, Methodology, Formal analysis, Data curation, Writing – review &
585 editing. **Luca Casettari:** Conceptualization, Resources, Funding acquisition, Project administration,
586 Supervision, Writing – review & editing.

587 Availability of data and materials

588 The datasets generated during and/or analysed during the current study are available from the
589 corresponding author on reasonable request.

590

591 Ethics approval and consent to participate

592 No animal or human studies were carried out by the authors for this article.

593 Consent for publication

594 No animal or human studies were carried out by the authors for this article.

595

596

597 **Compliance with ethical standards**

598 **Statement of Human and Animal Rights**

599 No animal or human studies were carried out by the authors for this article.

600 **Conflicts of Interest**

601 The authors declare that they have no conflict of interest

602

Journal Pre-proof

603 **Acknowledgements**

604 Graphical abstract was created using BioRender.

605

606

Journal Pre-proof

607 **References**

- 608 [1] Y. Thabet, V. Klingmann, J. Breitzkreutz, Drug Formulations: Standards and Novel Strategies
609 for Drug Administration in Pediatrics, *J Clin Pharmacol* 58 (2018).
610 <https://doi.org/10.1002/jcph.1138>.
- 611 [2] D. Khan, D. Kirby, S. Bryson, M. Shah, A. Rahman Mohammed, Paediatric specific dosage
612 forms: Patient and formulation considerations, *Int J Pharm* 616 (2022).
613 <https://doi.org/10.1016/j.ijpharm.2022.121501>.
- 614 [3] L. Rodríguez-Pombo, A. Awad, A.W. Basit, C. Alvarez-Lorenzo, A. Goyanes, Innovations in
615 Chewable Formulations: The Novelty and Applications of 3D Printing in Drug Product Design,
616 *Pharmaceutics* 14 (2022). <https://doi.org/10.3390/pharmaceutics14081732>.
- 617 [4] E. Villain, I. Denjoy, J.M. Lupoglazoff, P. Guicheney, B. Hainque, V. Lucet, D. Bonnet, Low
618 incidence of cardiac events with β -blocking therapy in children with long QT syndrome, *Eur*
619 *Heart J* 25 (2004). <https://doi.org/10.1016/j.ehj.2004.06.016>.
- 620 [5] E. Bidabadi, M. Mashouf, A Randomized Trial of Propranolol versus Sodium Valproate for the
621 Prophylaxis of Migraine in Pediatric Patients, *Pediatric Drugs* (2010).
622 <https://doi.org/10.2165/11316270-000000000-00000>.
- 623 [6] A.L. Marqueling, V. Oza, I.J. Frieden, K.B. Puttgen, Propranolol and infantile hemangiomas
624 four years later: A systematic review, *Pediatr Dermatol* 30 (2013) 182–191.
625 <https://doi.org/10.1111/pde.12089>.
- 626 [7] A. Lopalco, N. Denora, V. Laquintana, A. Cutrignelli, M. Franco, M. Robota, N. Hauschildt,
627 F. Mondelli, I. Arduino, A. Lopodota, Taste masking of propranolol hydrochloride by
628 microbeads of EUDRAGIT® E PO obtained with prilling technique for paediatric oral
629 administration, *Int J Pharm* 574 (2020). <https://doi.org/10.1016/j.ijpharm.2019.118922>.
- 630 [8] S. Castaneda, S. Melendez-Lopez, E. Garcia, H. De la Cruz, J. Sanchez-Palacio, The Role of
631 the Pharmacist in the Treatment of Patients with Infantile Hemangioma Using Propranolol,
632 *Adv Ther* 33 (2016). <https://doi.org/10.1007/s12325-016-0391-9>.
- 633 [9] H. Herrada-Manchón, D. Rodríguez-González, M. Alejandro Fernández, M. Suñé-Pou, P.
634 Pérez-Lozano, E. García-Montoya, E. Aguilar, 3D printed gummies: Personalized drug dosage
635 in a safe and appealing way, *Int J Pharm* 587 (2020).
636 <https://doi.org/10.1016/j.ijpharm.2020.119687>.
- 637 [10] V.M. Vaz, L. Kumar, 3D Printing as a Promising Tool in Personalized Medicine, *AAPS*
638 *PharmSciTech* 22 (2021). <https://doi.org/10.1208/s12249-020-01905-8>.
- 639 [11] P. Ganatra, L. Jyothish, V. Mahankal, T. Sawant, P. Dandekar, R. Jain, Drug-loaded vegan
640 gummies for personalized dosing of simethicone: A feasibility study of semi-solid extrusion-
641 based 3D printing of pectin-based low-calorie drug gummies, *Int J Pharm* 651 (2024).
642 <https://doi.org/10.1016/j.ijpharm.2024.123777>.

- 643 [12] EMA, Pharmaceutical development of medicines for paediatric use - Scientific guideline,
644 2013. [https://www.ema.europa.eu/en/pharmaceutical-development-medicines-paediatric-use-](https://www.ema.europa.eu/en/pharmaceutical-development-medicines-paediatric-use-scientific-guideline)
645 [scientific-guideline](https://www.ema.europa.eu/en/pharmaceutical-development-medicines-paediatric-use-scientific-guideline).
- 646 [13] J. Münch, A.L. Schwarzwälder, C. Kloft, H.M. Bosse, M. Wargenau, S. Reidemeister, I.
647 Klingmann, V. Klingmann, Validating a composite endpoint for acceptability evaluation of oral
648 drug formulations in the pediatric population: a randomized, open-label, single dose, cross-
649 over study, *Front Pharmacol* 15 (2024). <https://doi.org/10.3389/fphar.2024.1436554>.
- 650 [14] S.R. Ranmal, J. Walsh, C. Tuleu, Poor-tasting pediatric medicines: Part 1. A scoping review of
651 their impact on patient acceptability, medication adherence, and treatment outcomes, *Frontiers*
652 *in Drug Delivery* 5 (2025). <https://doi.org/10.3389/fddev.2025.1553286>.
- 653 [15] EMA, Formulations of Choice for the Paediatric Population - Scientific Guideline, 2005.
654 <http://www.emea.europa.eu>[https://www.ema.europa.eu/en/formulations-choice-paediatric-](https://www.ema.europa.eu/en/formulations-choice-paediatric-population-scientific-guideline)
655 [population-scientific-guideline](https://www.ema.europa.eu/en/formulations-choice-paediatric-population-scientific-guideline).
- 656 [16] I. El Aita, J. Rahman, J. Breikreutz, J. Quodbach, 3D-Printing with precise layer-wise dose
657 adjustments for paediatric use via pressure-assisted microsyringe printing, *European Journal*
658 *of Pharmaceutics and Biopharmaceutics* 157 (2020) 59–65.
659 <https://doi.org/10.1016/j.ejpb.2020.09.012>.
- 660 [17] M. Veselý, D. Záruba, J. Elbl, Development of 3D-Printed Chewable Gummy Tablets with
661 Adjustable Ondansetron Content for the Treatment of Pediatric Patients, *Pharmaceutics* 17
662 (2025). <https://doi.org/10.3390/pharmaceutics17040458>.
- 663 [18] K.J. Santamaría, B.J. Anaya, A. Lalatsa, P. González-Barranco, L. Cantú-Cárdenas, D.R.
664 Serrano, Engineering 3D Printed Gummies Loaded with Metformin for Paediatric Use, *Gels*
665 10 (2024). <https://doi.org/10.3390/gels10100620>.
- 666 [19] A. Imbriano, C. Fratini, G. Bondi, I. D’Abbrunzo, S. Bertoni, M. Tiboni, A. Abruzzo, D. Hasa,
667 C. Pagano, L. Casettari, 3D-printed chewable gummy tablets: A new tool for oral amoxicillin
668 administration in paediatric population, *Int J Pharm* 677 (2025).
669 <https://doi.org/10.1016/j.ijpharm.2025.125645>.
- 670 [20] T. Tagami, E. Ito, R. Kida, K. Hirose, T. Noda, T. Ozeki, 3D printing of gummy drug
671 formulations composed of gelatin and an HPMC-based hydrogel for pediatric use, *Int J Pharm*
672 594 (2021). <https://doi.org/10.1016/j.ijpharm.2020.120118>.
- 673 [21] A. Dalmoro, A.A. Barba, G. Lamberti, M. Grassi, M. D’Amore, Pharmaceutical applications
674 of biocompatible polymer blends containing sodium alginate, *Advances in Polymer*
675 *Technology* 31 (2012) 219–230. <https://doi.org/10.1002/adv.21276>.
- 676 [22] J. Liu, X. Zhan, J. Wan, Y. Wang, C. Wang, Review for carrageenan-based pharmaceutical
677 biomaterials: Favourable physical features versus adverse biological effects, *Carbohydr Polym*
678 121 (2015) 27–36. <https://doi.org/10.1016/j.carbpol.2014.11.063>.
- 679 [23] N. Grizzuti, G. Buonocore, G. Iorio, Viscous behavior and mixing rules for an immiscible
680 model polymer blend, *J Rheol* (2000). <https://doi.org/10.1122/1.551073>.

- 681 [24] H. Herrada-Manchón, M.A. Fernández, E. Aguilar, Essential Guide to Hydrogel Rheology in
682 Extrusion 3D Printing: How to Measure It and Why It Matters?, *Gels* 9 (2023).
683 <https://doi.org/10.3390/gels9070517>.
- 684 [25] H. Xu, Q. Fan, M. Huang, L. Cui, Z. Gao, L. Liu, Y. Chen, J. Jin, Q. Jin, X. Wang, Combination
685 of carrageenan with sodium alginate, gum arabic, and locust bean gum: Effects on rheological
686 properties and quiescent stabilities of partially crystalline emulsions, *Int J Biol Macromol* 253
687 (2023). <https://doi.org/10.1016/j.ijbiomac.2023.127561>.
- 688 [26] P. Adão, M. da L. Calado, W. Fernandes, L.G. Alves, L. Côrte-Real, M. Guedes, R. Baptista,
689 R. Bernardino, M.M. Gil, M.J. Campos, S. Bernardino, Use of Limestone Sludge in the
690 Preparation of ι-Carrageenan/Alginate-Based Films, *Materials* 17 (2024).
691 <https://doi.org/10.3390/ma17071668>.
- 692 [27] A. Tziboula, D.S. Horne, Influence of milk proteins on-carrageenan gelation, *Int Dairy J*
693 (1999). [https://doi.org/10.1016/S0958-6946\(99\)00088-6](https://doi.org/10.1016/S0958-6946(99)00088-6).
- 694 [28] D.A. Rau, M.J. Bortner, C.B. Williams, A rheology roadmap for evaluating the printability of
695 material extrusion inks, *Addit Manuf* 75 (2023). <https://doi.org/10.1016/j.addma.2023.103745>.
- 696 [29] M.A. Habib, B. Khoda, Rheological analysis of bio-ink for 3D bio-printing processes, *J Manuf*
697 *Process* 76 (2022). <https://doi.org/10.1016/j.jmapro.2022.02.048>.
- 698 [30] I. Insua, O. Etzold, I. Calafel, R. Aguirresarobe, M. Calderón, M. Fernández, Rheological
699 Insight into the 3D Printability of Carboxymethyl Cellulose-Based Hydrogels, *Gels* 11 (2025).
700 <https://doi.org/10.3390/gels11040259>.
- 701 [31] C. Fratini, E. Weaver, S. Moroni, R. Irwin, Y.H. Dallal Bashi, S. Uddin, L. Casettari, M.P.
702 Wylie, D.A. Lamprou, Combining microfluidics and coaxial 3D-bioprinting for the
703 manufacturing of diabetic wound healing dressings, *Biomaterials Advances* 153 (2023).
704 <https://doi.org/10.1016/j.bioadv.2023.213557>.
- 705 [32] Z. Noralian, M.P. Gashti, M.R. Moghaddam, H. Tayyeb, I. Erfanian, Ultrasonically developed
706 silver/iota-carrageenan/cotton bionanocomposite as an efficient material for biomedical
707 applications, *Int J Biol Macromol* 180 (2021). <https://doi.org/10.1016/j.ijbiomac.2021.02.204>.
- 708 [33] Y.Q. Wang, Y.T. Han, J.N. Yan, Y.N. Du, X.Y. Jiang, H.T. Wu, Gel properties and network
709 structure of the hydrogel constructed by iota-carrageenan and Ala-Lys dipeptide, *Int J Biol*
710 *Macromol* 182 (2021). <https://doi.org/10.1016/j.ijbiomac.2021.04.001>.
- 711 [34] O.M. Amin, H.N. EL Qady, M.A. Abd El-Fattah, An Intragastric Delivery Device Employing
712 FDM Technology: 3D-Printed Tablet Containing Green Developed Mosapride-Saccharin Co-
713 crystals, *AAPS PharmSciTech* 24 (2023). <https://doi.org/10.1208/s12249-023-02578-9>.
- 714 [35] S. Bandari, V.R. Dronam, B.B. Eedara, Development and preliminary characterization of
715 levofloxacin pharmaceutical cocrystals for dissolution rate enhancement, *J Pharm Investig* 47
716 (2017). <https://doi.org/10.1007/s40005-016-0302-8>.

- 717 [36] S. Salehi, S. Boddohi, Design and optimization of kollicoat® IR based mucoadhesive buccal
718 film for co-delivery of rizatriptan benzoate and propranolol hydrochloride, *Materials Science*
719 *and Engineering C* 97 (2019). <https://doi.org/10.1016/j.msec.2018.12.036>.
- 720 [37] A. Gangopadhyay, R. Saha, A. Bose, R.N. Sahoo, S. Nandi, R. Swain, M. Paul, S. Biswas, R.
721 Mohapatra, Effect of annealing time on the applicability of potato starch as an excipient for
722 the fast disintegrating propranolol hydrochloride tablet, *J Drug Deliv Sci Technol* 67 (2022).
723 <https://doi.org/10.1016/j.jddst.2021.103002>.
- 724 [38] D.A.V. Medina, A.P.G. Ferreira, E.T.G. Cavalheiro, Thermal investigation on polymorphism
725 in sodium saccharine, *J Therm Anal Calorim* 117 (2014). [https://doi.org/10.1007/s10973-014-](https://doi.org/10.1007/s10973-014-3733-3)
726 [3733-3](https://doi.org/10.1007/s10973-014-3733-3).
- 727 [39] S. Bhatia, A. Al-Harrasi, Y.A. Shah, M. Jawad, M.S. Al-Azri, S. Ullah, M.K. Anwer, M.F.
728 Aldawsari, E. Koca, L.Y. Aydemir, Physicochemical Characterization and Antioxidant
729 Properties of Chitosan and Sodium Alginate Based Films Incorporated with Ficus Extract,
730 *Polymers* 15 (2023). <https://doi.org/10.3390/polym15051215>.
- 731 [40] M. Bartolomei, P. Bertocchi, M.C. Ramusino, E.C. Signoretti, Thermal studies on the
732 polymorphic modifications of (R,S) propranolol hydrochloride, *Thermochimica Acta* (1998).
733 [https://doi.org/10.1016/S0040-6031\(98\)00438-9](https://doi.org/10.1016/S0040-6031(98)00438-9).
- 734 [41] J. Fang, X. Chen, Q. Xiao, Y. Zhang, H. Weng, J. Chen, Q. Yang, F. Chen, A. Xiao, Structure
735 transition and gel melioration of ι -carrageenan and non-gelling senna tora gum mixed gel, *Int*
736 *J Biol Macromol* 320 (2025). <https://doi.org/10.1016/j.ijbiomac.2025.145790>.
- 737 [42] K. Prasad, Y. Kaneko, J.I. Kadokawa, Novel gelling systems of κ -, ι - and λ - carrageenans and
738 their composite gels with cellulose using ionic liquid, *Macromol Biosci* 9 (2009).
739 <https://doi.org/10.1002/mabi.200800179>.
- 740 [43] S.F. Mohseni-Motlagh, R. Dolatabadi, M. Baniassadi, M. Karimpour, M. Baghani, Tablet
741 Geometry Effect on the Drug Release Profile from a Hydrogel-Based Drug Delivery System,
742 *Pharmaceutics* 15 (2023). <https://doi.org/10.3390/pharmaceutics15071917>.
- 743 [44] M.P. Paarakh, P. Ani Jose, C. Setty, G. Peter Christopher, Release Kinetics - Concepts and
744 Applications, *Int J Pharm Research and Tech* (2018).
745 <https://doi.org/doi.org/10.31838/ijprt/08.01.02>.
- 746 [45] E.A. Pinto, J.L. Dávila, M.A. d'Ávila, Rheological studies on nanocrystalline
747 cellulose/alginate suspensions, *J Mol Liq* 277 (2019).
748 <https://doi.org/10.1016/j.molliq.2018.12.091>.
- 749 [46] M.I. Calafel, M. Criado-Gonzalez, R. Aguirresarobe, M. Fernández, C. Mijangos, From
750 rheological concepts to additive manufacturing assessment of hydrogel-based materials for
751 advanced bioprinting applications, *Mater Adv* 6 (2025). <https://doi.org/10.1039/d5ma00019j>.
- 752 [47] R. V. Kulkarni, V. V. Baraskar, C. Mallikarjun Setty, S. Biswanath, Interpenetrating Polymer
753 Network Matrices of Sodium Alginate and Carrageenan for Controlled Drug Delivery
754 Application, *Fibers and Polymers* (2011). <https://doi.org/10.1007/s12221-011-0352-5>.

- 755 [48] C. Croitoru, I.C. Roata, A. Pascu, E.M. Stanciu, Diffusion and controlled release in physically
756 crosslinked poly (vinyl alcohol)/iota-carrageenan hydrogel blends, *Polymers* 12 (2020).
757 <https://doi.org/10.3390/polym12071544>.
- 758 [49] F. Zhang, L. Lin, Z. Wang, H. Li, Evaluation, correction and masking methods for unpleasant
759 tastes of drugs: A comprehensive review, *Int J Pharm* (2025).
760 <https://doi.org/10.1016/j.ijpharm.2025.126008>.
- 761 [50] M. Roelse, N. Krasteva, S. Pawlizak, M.K. Mai, M.A. Jongsma, Tongue-on-a-Chip: Parallel
762 Recording of Sweet and Bitter Receptor Responses to Sequential Injections of Pure and Mixed
763 Sweeteners, *J Agric Food Chem* 72 (2024) 15854–15864.
764 <https://doi.org/10.1021/acs.jafc.4c00815>.
- 765 [51] L. Castle, M. Andreassen, G. Aquilina, M.L. Bastos, P. Boon, B. Fallico, R. FitzGerald, M.J.F.
766 Fernandez, B. Grasl-Kraupp, U. Gundert-Remy, R. Gürtler, E. Houdeau, M. Kurek, H. Louro,
767 P. Morales, S. Passamonti, M. Batke, E. Bruzell, J. Chipman, K. Cheyins, R. Crebelli, C. Fortes,
768 P. Fürst, T. Halldorsson, J.C. LeBlanc, M. Mirat, O. Lindtner, A. Mortensen, E. Ntzani, R.
769 Shah, H. Wallace, M. Wright, S. Barmaz, C. Civitella, P. Georgelova, F. Lodi, E. Mazzoli, J.
770 Rasinger, A.M. Rincon, A. Tard, P. Zakidou, M. Younes, Re-evaluation of saccharin and its
771 sodium, potassium and calcium salts (E 954) as food additives, *EFSA Journal* 22 (2024).
772 <https://doi.org/10.2903/j.efsa.2024.9044>.
- 773 [52] H. Herrada-Manchón, D. Rodríguez-González, M. Alejandro Fernández, M. Suñé-Pou, P.
774 Pérez-Lozano, E. García-Montoya, E. Aguilar, 3D printed gummies: Personalized drug dosage
775 in a safe and appealing way, *Int J Pharm* 587 (2020).
776 <https://doi.org/10.1016/j.ijpharm.2020.119687>.
- 777 [53] J. Long, A. Nand, S. Ray, Application of spectroscopy in additive manufacturing, *Materials* 14
778 (2021). <https://doi.org/10.3390/MA14010203>.
- 779 [54] A. Abdollahi, Z. Ansari, M. Akrami, I. Haririan, S. Dashti-Khavidaki, M. Irani, M. Kamankesh,
780 E. Ghobadi, Additive Manufacturing of an Extended-Release Tablet of Tacrolimus, *Materials*
781 16 (2023). <https://doi.org/10.3390/ma16144927>.
- 782 [55] C. Bendicho-Lavilla, L. Rodríguez-Pombo, P. Januskaite, C. Rial, C. Alvarez-Lorenzo, A.W.
783 Basit, A. Goyanes, Ensuring the quality of 3D printed medicines: Integrating a balance into a
784 pharmaceutical printer for in-line uniformity of mass testing, *J Drug Deliv Sci Technol* 92
785 (2024). <https://doi.org/10.1016/j.jddst.2024.105337>.
- 786 [56] C.J. Parramon-Teixido, L. Rodríguez-Pombo, A.W. Basit, A. Worsley, C. Cañete-Ramírez, C.
787 Alvarez-Lorenzo, M.J. Cabañas-Poy, A. Goyanes, A framework for conducting clinical trials
788 involving 3D printing of medicines at the point-of-care, *Drug Deliv Transl Res* (2025).
789 <https://doi.org/10.1007/s13346-025-01868-y>.

790

791

792 **Table 1.** Hydrogel formulations containing 4 % w/w of propranolol hydrochloride (PR_{HCl}).

793 Percentages are all expressed in w/w.

794 **Table 2.** Setting parameters for the three interval thixotropy test (3ITT).

795 **Table 3.** Summarizing table showing the average real dimensions (measured with a digital calliper

796 Mitutoyo, Japan), printing time, weight and drug content for the four 3D printed dosage units.

797 **Table 4.** Calculated mechanical parameters for the 3D-printed *gummies* vs commercially available

798 *gummies*.

799

800

801

802

Journal Pre-proof

803 **Table 1.** Hydrogel formulations containing 4 % w/w of propranolol hydrochloride (PR_{HCl}).

804 Percentages are all expressed in w/w.

Formulation	SA	t-K	E954
F1	10%	0%	0.5%
F2	5%	5%	0.5%
F3	4%	6%	0.5%
F4	3%	7%	0.5%
F5	0%	10%	0.5%

805

806

Table 2. Setting parameters for the three interval thixotropy test (3ITT).

Step	Shear rate (s⁻¹)	Time interval (seconds)
1	1, constant	120
2	100 - 1000, logarithmic ramp	320
3	1, constant	120

807

Journal Pre-proof

808 **Table 3.** Summarizing table showing the average real dimensions (measured with a digital calliper
809 Mitutoyo, Japan), printing time, weight and drug content for the four 3D printed dosage units.

CAD dimensions (mm)	Real dimensions (mm)	Printing time (min)	Weight (mg)	Drug content (mg)
15x15x5	14.96x14.95x5.22	12	991.55 ± 8.54	40.04 ± 1.35
12x12x4	12.18x12.12x4.1	8	608.98 ± 5.76	24.36 ± 0.63
10x10x3	10.15x10.09x3.14	4	331.25 ± 5.37	13.25 ± 0.71
8x8x2	8.02x7.99x2.10	1.5	110.75 ± 3.59	4.43 ± 0.15

810

811

812 **Table 4.** Calculated mechanical parameters for the 3D-printed *gummies* vs commercially available
813 *gummies*.

Sample	Hardness (N)	Cohesiveness	Chewiness (N)
3D-printed <i>gummies</i>	27.51 ± 3.72	0.41 ± 0.03	11.22 ± 1.48
Marketed <i>gummies</i>	47.44 ± 1.76	0.88 ± 0.02	43.57 ± 3.77

814

Journal Pre-proof

815 **Figure 1:** Comparison of the calculated and experimental viscosities of the tested formulations
816 (expressed as the natural logarithm). Positive deviation for the experimental values respect to the
817 theoretical ones underlining the miscibility of the polymers (A); negative deviation from the
818 theoretical values occurring when propranolol is added to the formulation (B).

819 **Figure 2:** A) Flow curves, showing the shear thinning behaviour of the formulations; B) Three-
820 interval thixotropy test (3ITT), showing the recovery of the formulation's viscosity after the three
821 shear stages. Amplitude sweeps of the tested formulations both unloaded (C) and loaded with the
822 API (D); Frequency sweeps of the tested formulations both unloaded (E) and loaded with the API

823 **Figure 3:** A) Visual comparison of the behaviour of the tested formulations at the 3D printer
824 showing the shape of the extruded material, and the top and lateral view of the 3D-printed *gummies*;
825 B) CAD design of the 3D-printed *gummy*; C) Images of the 3D-printed *gummy* at the optical
826 microscope after cross-linking showing the top (left) and lateral side of the final dosage form
827 (right); D) 3D printing of different dimensions of the dosage unit to achieve different drug loading
828 demonstrating the versatility of the manufacturing process.

829 **Figure 4:** (A) FTIR spectra of the raw materials: SA (a), ι -K (b), E954 (c), PR_{HCl} (f) compared to
830 the unloaded 3D-printed *gummy* (d) and loaded 3D-printed *gummies* (e); (B) FTIR spectra showing
831 the homogeneous distribution of PR_{HCl} in the 3D-printed *gummies*; C) Distribution spectral map
832 evaluating the signal intensities at 1105 cm⁻¹ and 769 cm⁻¹ and representing the drug distribution in
833 three different pieces of a single dosage unit (A, B, C) and in three different units (Sample1,
834 Sample 2, Sample 3) chosen randomly.

835 **Figure 5:** Solid state characterization of the 3D-printed *gummies* and starting raw materials at the
836 (A) DSC, (B) TGA, and (C) PXRD.

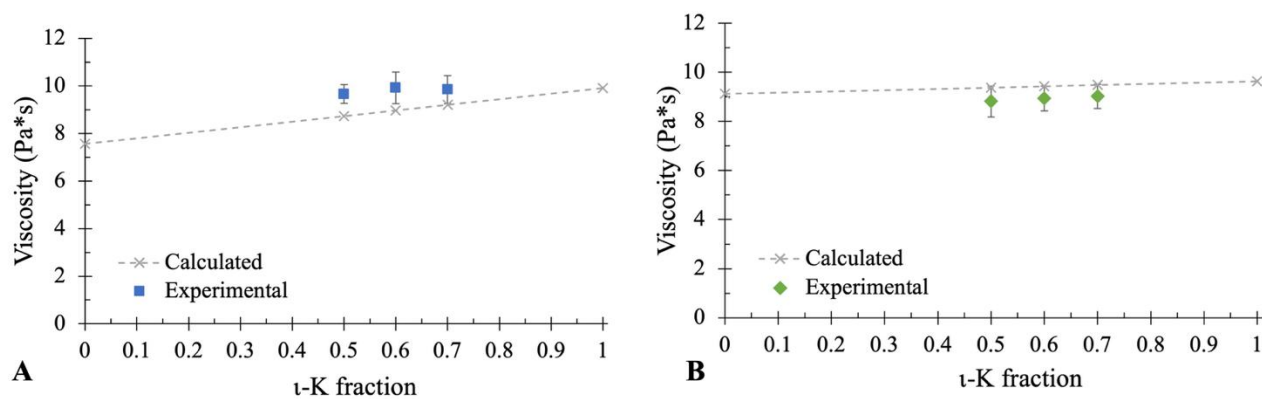
837 **Figure 6:** Distribution of single dosage forms' weights around the average (A) and of single dosage
838 forms' content around the average (B) within the limits given by the European Pharmacopoeia. (C)

839 Cumulative drug release profile of PR_{HCl} from the 3D-printed *gummies* with different design
840 dimensions (15x15x5 mm, 12x12x4 mm, 10x10x3 mm, 8x8x2 mm).

841 **Figure 7:** (A) Texture profile analysis of the 3D-printed *gummies* vs marketed gummies. (B)
842 Average water content and mass loss of the 3D-printed *gummies* through 7-days period under
843 packaging conditions. Trends of hardness (C), cohesiveness (D), and gumminess (E) of the 3D-
844 printed *gummies* through 7-days period under packaging conditions.

845

Journal Pre-proof

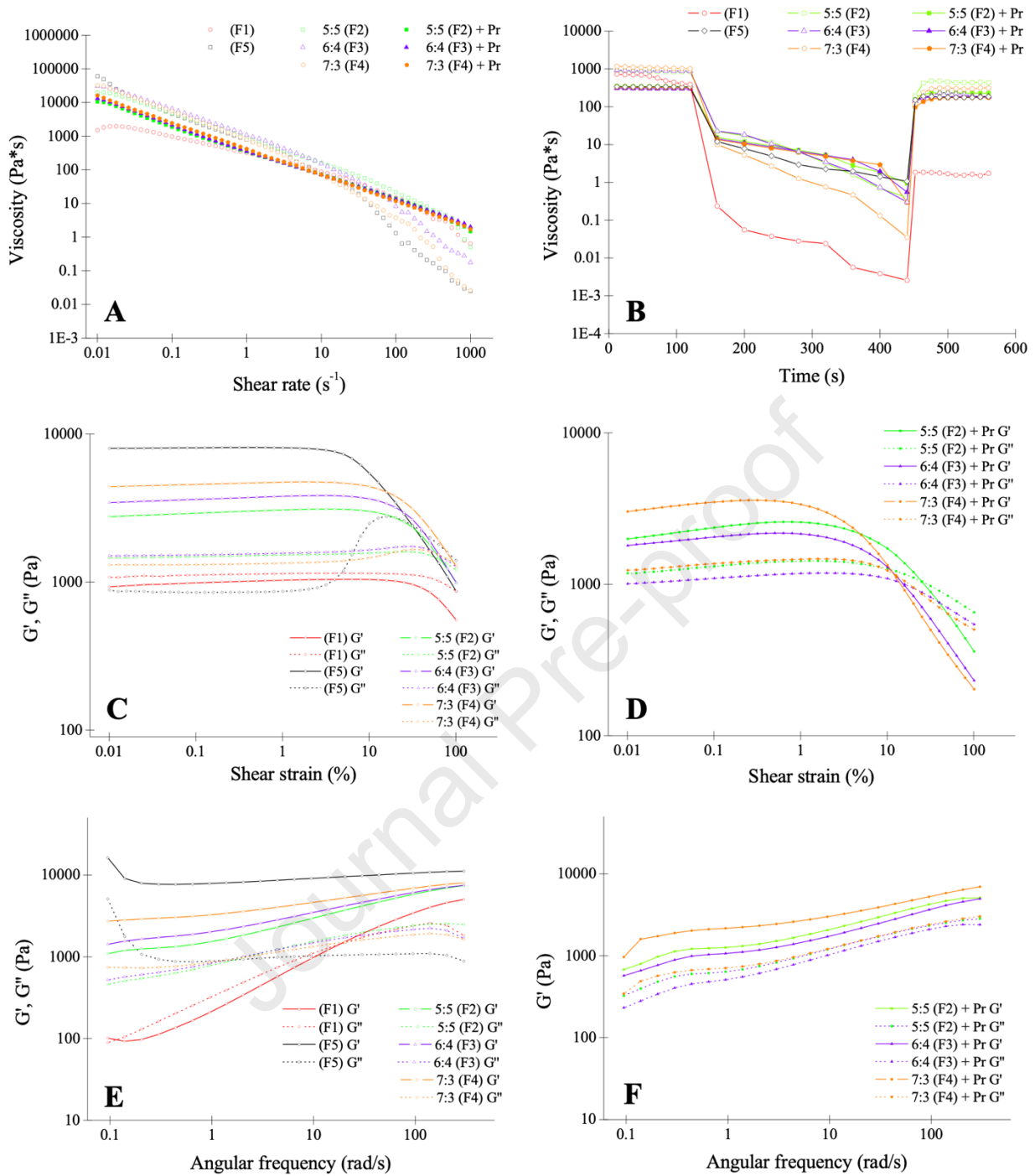


846

847 **Figure 1:** Comparison of the calculated and experimental viscosities of the tested formulations
848 (expressed as the natural logarithm). Positive deviation for the experimental values respect to the
849 theoretical ones underlining the miscibility of the polymers (A); negative deviation from the
850 theoretical values occurring when propranolol is added to the formulation (B).

851

852



853

854

855

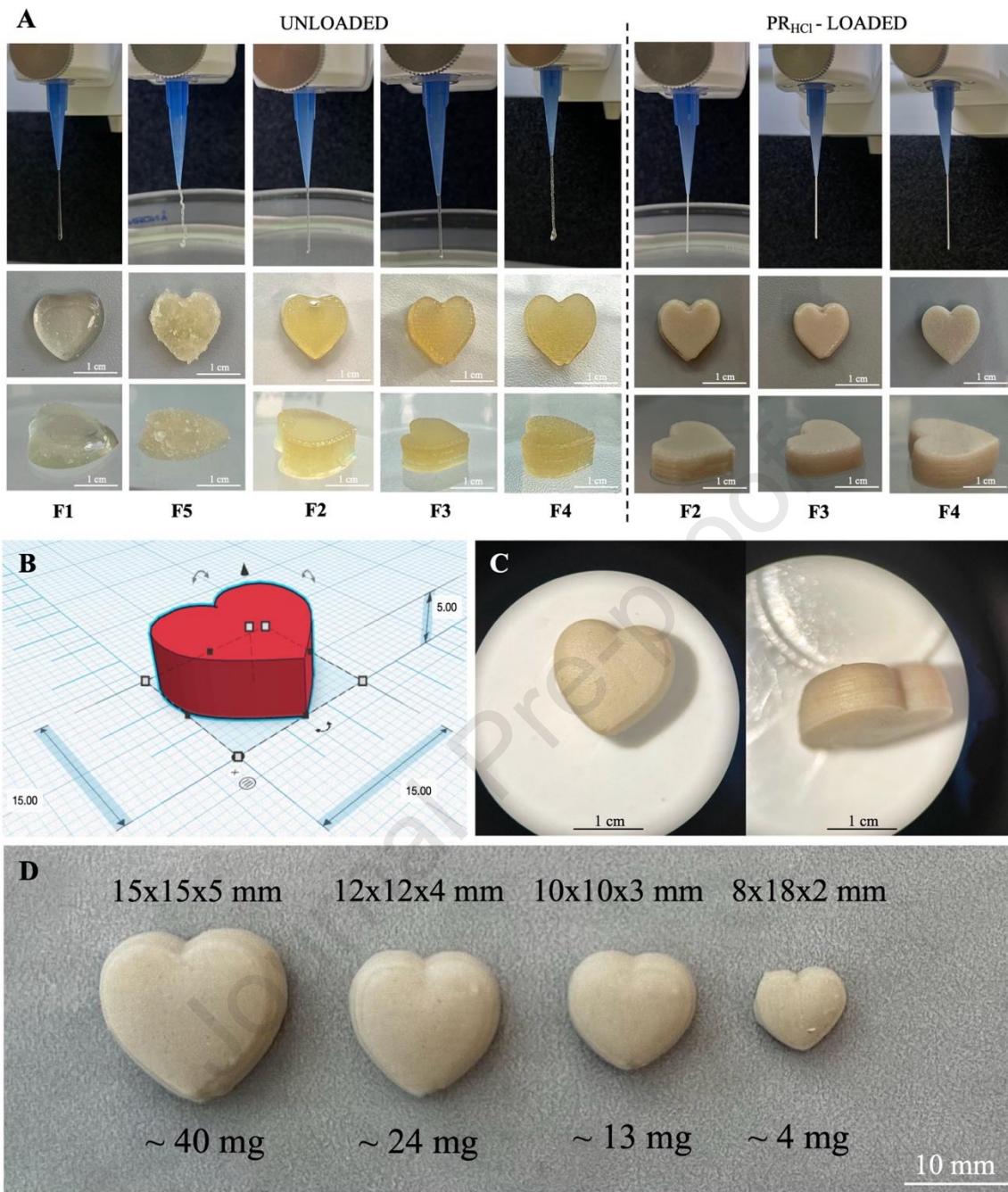
856

857

858

859

Figure 2: A) Flow curves, showing the shear thinning behaviour of the formulations; B) Three-interval thixotropy test (3ITT), showing the recovery of the formulation's viscosity after the three shear stages. Amplitude sweeps of the tested formulations both unloaded (C) and loaded with the API (D); Frequency sweeps of the tested formulations both unloaded (E) and loaded with the API (F).



860

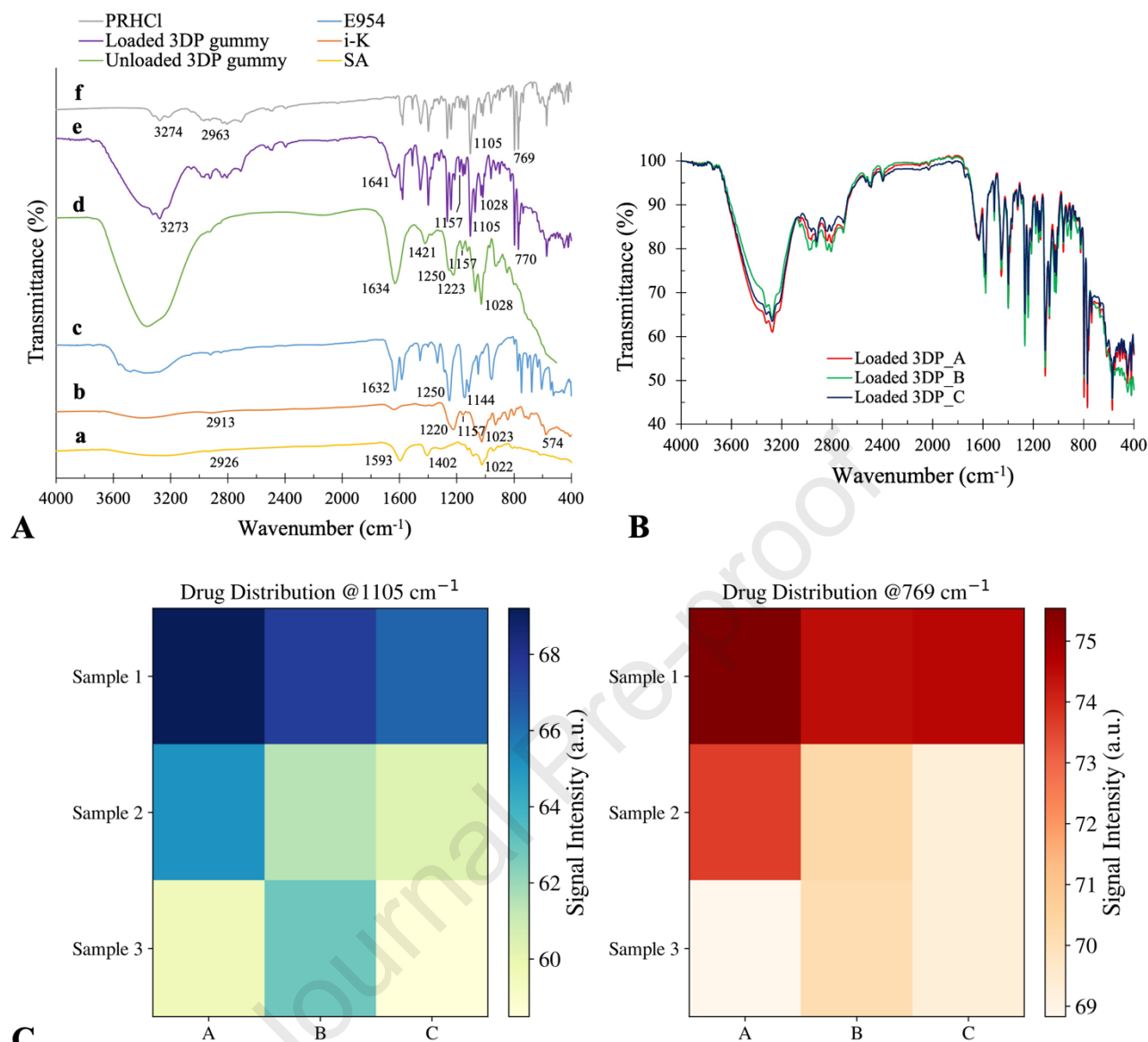
861 **Figure 3:** A) Visual comparison of the behaviour of the tested formulations at the 3D printer
 862 showing the shape of the extruded material, and the top and lateral view of the 3D-printed *gummies*;

863 B) CAD design of the 3D-printed *gummy*; C) Images of the 3D-printed *gummy* at the optical
 864 microscope after cross-linking showing the top (left) and lateral side of the final dosage form

865 (right); D) 3D printing of different dimensions of the dosage unit to achieve different drug loading

866 demonstrating the versatility of the manufacturing process.

867



868

869

870

871

872

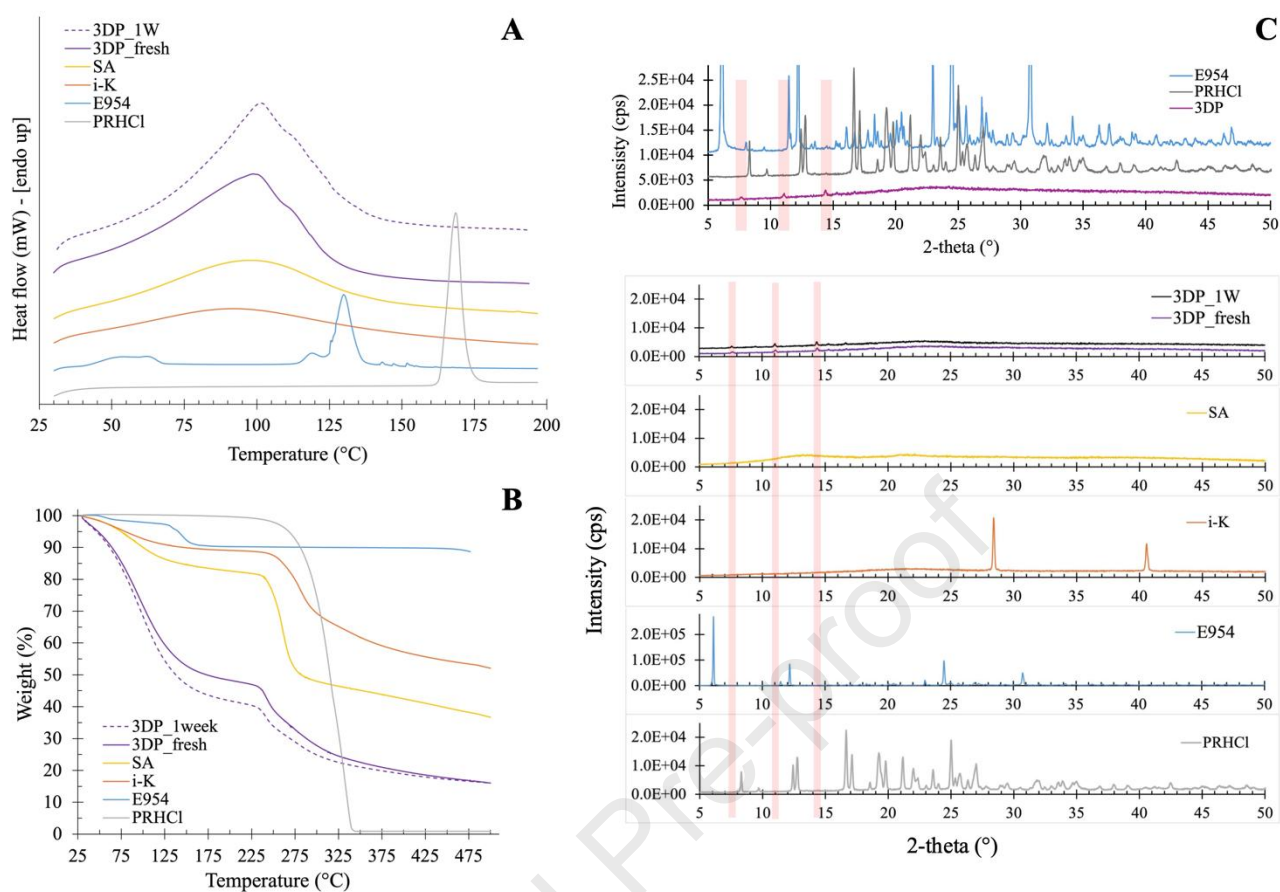
873

874

875

876

Figure 4: (A) FTIR spectra of the raw materials: SA (a), t-K (b), E954 (c), PR_{HCl} (f) compared to the unloaded 3D-printed *gummy* (d) and loaded 3D-printed *gummies* (e); (B) FTIR spectra showing the homogeneous distribution of PR_{HCl} in the 3D-printed *gummies*; (C) Distribution spectral map evaluating the signal intensities at 1105 cm^{-1} and 769 cm^{-1} and representing the drug distribution in three different pieces of a single dosage unit (A, B, C) and in three different units (Sample1, Sample 2, Sample 3) chosen randomly.



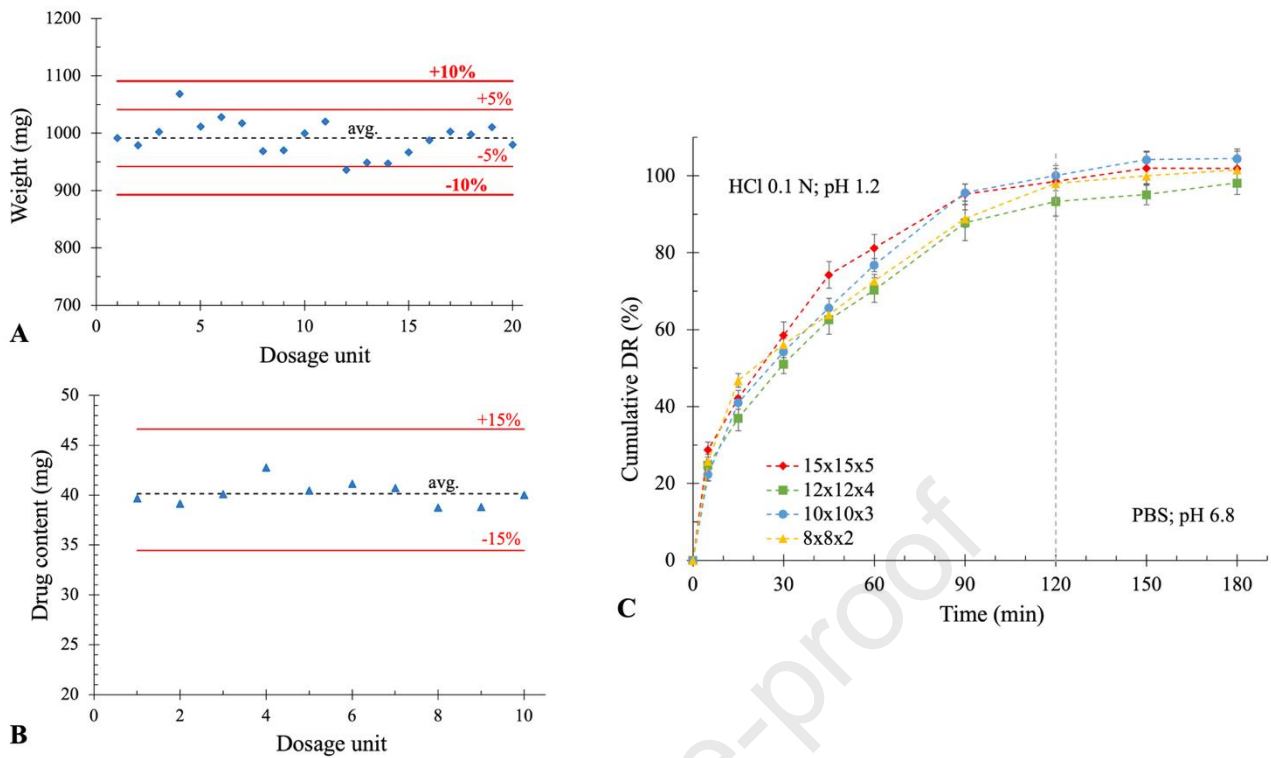
877

878

879

880

Figure 5: Solid state characterization of the 3D-printed *gummies* and starting raw materials at the (A) DSC, (B) TGA, and (C) PXR D.

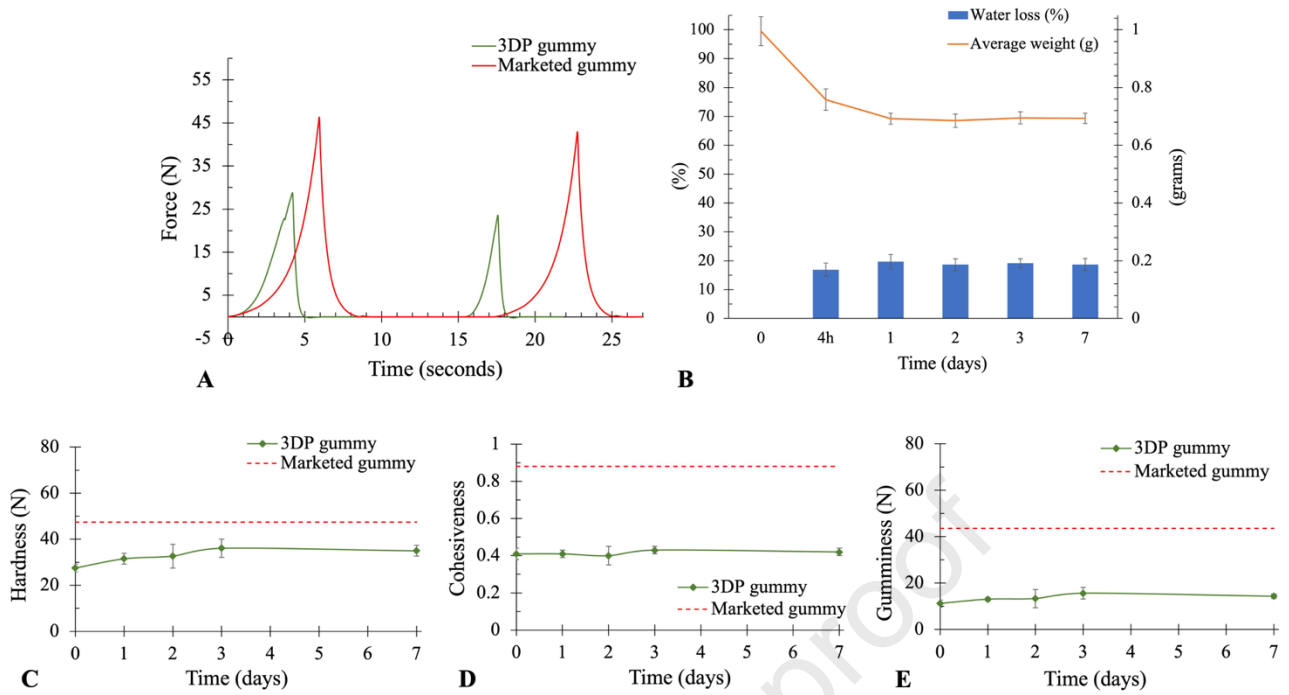


881

882 **Figure 6:** Distribution of single dosage forms' (15x15x5 mm) weights around the average (A) and
 883 of single dosage forms' content around the average (B) within the limits given by the European
 884 Pharmacopoeia. (C) Cumulative drug release profile of PR_{HCl} from the 3D-printed *gummies* with
 885 different design dimensions (15x15x5 mm, 12x12x4 mm, 10x10x3 mm, 8x8x2 mm).

886

887



888

889 **Figure 7:** (A) Texture profile analysis of the 3D-printed *gummies* vs marketed *gummies*. (B)890 Average water content and mass loss of the 3D-printed *gummies* through 7-days period under

891 packaging conditions. Trends of hardness (C), cohesiveness (D), and gumminess (E) of the 3D-

892 printed *gummies* through 7-days period under packaging conditions.

893

894



Declaration of Interest Statement

The authors declare that they have no known competing financial interests or personal relationships that could have appeared to influence the work reported in this paper.

Mattia Tiboni, PhD

University of Urbino Carlo Bo

Department of Biomolecular Sciences -

School of Pharmacy

Campus Scientifico "Enrico Mattei"

61029 Urbino (PU) – Italy

web site: www.pharmatech.uniurb.it

mattia.tiboni@uniurb.it

office: +39(0)722303336